

# Seismic wave propagation in icy ocean worlds

Simon C. Stähler<sup>1,2,\*</sup>, Mark P. Panning<sup>3,†</sup>, Steve D. Vance<sup>4</sup>, Ralph Lorenz<sup>5</sup>, Martin van Driel<sup>6</sup>,  
Tarje Nissen-Meyer<sup>7</sup>, Sharon Kedar<sup>4</sup>

<sup>1</sup>Ludwig-Maximilians-Universität München, Geophysik

<sup>2</sup>Leibniz-Institute for Baltic Sea Research, Rostock, Germany

<sup>3</sup>University of Florida, Gainesville, USA

<sup>4</sup>Jet Propulsion Laboratory, California Institute of Technology, Pasadena, USA

<sup>5</sup>Johns Hopkins University Applied Physics Laboratory, Laurel, USA

<sup>6</sup>Institute for Geophysics, ETH Zürich, Switzerland

<sup>7</sup>Department of Earth Sciences, University of Oxford, United Kingdom

## Key Points:

- Prepares for icy moon seismology by proposing a phase name scheme
- Observation of a few M3 events allows estimates of ice thickness and ocean depth
- The existence of high-pressure ice phases can be inferred from spectral analysis

arXiv:1705.03500v1 [physics.geo-ph] 9 May 2017

---

\*now at ETH Zürich, Institute for Geophysics

†now at JPL

Corresponding author: Simon Stähler, [mail@simonstaehler.com](mailto:mail@simonstaehler.com)

## Abstract

To date, seismological efforts have been limited to terrestrial objects: Earth, the Moon, and soon Mars. All have in common a rigid lithosphere above a solid mantle. The coming years may see the development of seismological experiments for Europa, Titan and Enceladus, so it is necessary to adapt seismological concepts to the setting of worlds with global oceans covered in ice. Here we use wave form analyses to identify and classify wave types, developing a lexicon for icy ocean world seismology intended to be useful to both seismologists and planetary scientists. We use results from spectral-element simulations of broadband seismic wavefields to adapt seismological concepts to icy ocean worlds. We present a concise naming scheme for seismic waves and an overview over the features of the seismic wavefield on Europa, Titan, Ganymede and Enceladus. In close connection with geophysical interior models, we analyze simulated seismic measurements of Europa and Titan that might be used to constrain geochemical parameters governing the habitability of a sub-ice ocean.

## 1 Introduction

The largest icy moons of the solar system’s gas planets probably harbour liquid oceans below their surface [Nimmo and Pappalardo, 2016]. These oceans have been predicted from the estimated internal energy budget by radioactive decay and tides [Lewis, 1971; Cassen *et al.*, 1979], the density structure inferred from gravitational moment-of-inertia measurements, tectonic interpretations of the ice thickness, and electromagnetic effects consistent with conductive fluids beneath the ice [Kivelson *et al.*, 2000]. Due to the low density contrasts and ambiguity of electrical conductance measurements, these methods alone cannot constrain the thicknesses of ice and ocean layers uniquely, which are crucial to the ocean chemistry and therefore habitability. Especially in the large worlds Ganymede, Callisto and Titan, high-pressure ice phases could act as a material barrier between rocky mantle and ocean [Vance *et al.*, 2014], with a potentially negative effect on habitability. Briny fluids [Hogenboom *et al.*, 1995] or ice convection might mitigate this effect [Choblet *et al.*, 2017], nevertheless the presence, structure and dynamics of these ices is therefore of great scientific interest.

The thickness of a surface ice layer below a few kilometers can be estimated from radar measurements, as planned for the upcoming ESA JUICE and NASA Europa Clipper missions [Bruzzone *et al.*, 2013; Phillips and Pappalardo, 2014]. However, due to the low impedance contrast between ice and liquid water, uncertainty may be high. Attenuation in the water will make it difficult to impossible to measure the ocean depth with radar. Seismological measurements could ideally complement the existing methods. Where radar is sensitive to electrical conductivity, and crystal orientation fabric (COF), seismic waves are influenced by elastic parameters and indirectly by material chemistry, COF, and temperature [Diez, 2013]. A detailed discussion of geophysical measurements linked to habitability can be found in the companion paper by Vance *et al.* [2017].

The seismology of an icy ocean world is rather different from the one on Earth and many of the classical concepts and terminology of seismology make little sense and need to be re-thought. The global ocean with its low seismic velocity and absence of S-waves decouples the seismic wavefield in the ice and the mantle, creating seismic wave types that are not observed on a global scale on Earth. The coming decades will likely bring the first seismological station on an icy moon [Hand *et al.*, 2017], and mission design begins now. This paper gives an introduction to the general features of icy ocean world seismology, which should help terrestrial seismologists adapt their vocabulary and thinking to this environment. With the possibility of landers on Europa, Titan and Enceladus in the next decade or two, these three worlds are discussed in more detail. Ganymede is discussed as an end-member in size and ocean thickness. To keep the paper concise, we will not discuss Callisto and potential ocean worlds in the Uranus and Neptune systems in detail, even though the general concepts

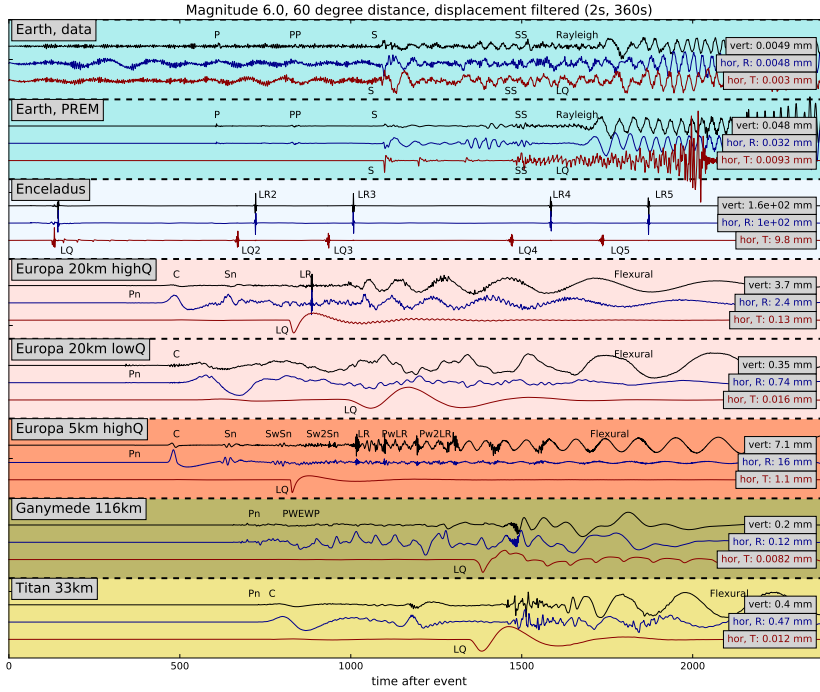


**Figure 1.** Comparison of a measured seismograms on Earth (Earthquake in the Lake Tanganyika region on 2016/02/24, 32 km depth; measured at BFO in Southern Germany in 60 degree epicentral distance) with synthetic seismograms for Earth, Enceladus, Europa, Ganymede and Titan with equivalent source-receiver distance. The source model is the real moment tensor [*Global CMT Project, 2017, gcmtdid:C201702240032A*], with a source duration of 2 seconds. For the icy moons, the depth has been reduced to 3 km, to ensure that the event is in the ice. The black line is the vertical motion, red is radial (horizontal, pointing away from the event), and blue is horizontal transverse, perpendicular to R.

The measured seismogram on Earth is different from the PREM reference synthetic [*Dziewoński and Anderson, 1981*], since the surface waves travelled along a path through thick continental crust, while PREM contains an oceanic, thin-crust model. To a seismologist, the waveform fit looks reasonable, but it is obvious that no simple global reference model can explain the complete shape of the seismic waveform. Also note the presence of ocean-generated microseismic noise in the data with periods of 7 seconds and another noise signal of around 100s period. This difference may give an idea on what the difference between the predicted signals for the icy worlds and a real signal there might be.

It is immediately obvious that the seismograms on icy worlds contain unknown phases, especially the prominent long-period flexural waves in the ice and a strong, non-dispersive phase on the R-component (Crary phase). On Enceladus, the Rayleigh (on Z and R) and Love (on T) surface waves take around 800 seconds to orbit the moon and they are little attenuated. The seismogram is therefore dominated by its repeated occurrences, which will allow to determine the distance between an Enceladusquake and the receiver [for an application to Mars, see *Panning et al., 2015*]. On Europa, the ice layer is so thin that amplitude and shape of the seismogram depends very strongly on the thickness of the ice layer. On Ganymede, with a 116km ice layer, the overall seismogram shares many features with the Earth: Body waves with low amplitudes arrive first, followed by a complex surface wave train, but very weak exotic phases.

presented here apply to them as well. For the four worlds, potential seismic tests for habitability are presented and tested using synthetic seismograms.

Previous studies of seismology on Europa are mostly older than a decade and were therefore limited to the computational methods of the time. The very detailed study of [Kovach and Chyba, 2001] was mainly based on ray-theoretical methods and analytic derivations and did not calculate any full seismograms, Lee and Ben-Zion [2006] used ray theory for the ice and ocean layer only, Panning *et al.* [2006] used the normal mode method [Woodhouse, 1988] to calculate seismograms, but were limited to long periods (>10s), where some of the ice layer effects are not visible yet. Computational seismology has progressed rapidly in the last decade [for an overview, see Igel, 2017], which allows for a full modeling of the broadband global wavefield for the first time now. We used the spectral-element solver *AxiSEM* [Nissen-Meyer *et al.*, 2014], which is extremely efficient for layered models, since it reduces the 3D wave propagation to a 2D problem. A second companion paper [Panning *et al.*, 2017], uses this method and a seismicity model to estimate the seismic background noise caused by tidal cracking on Europa.

Figure 1 shows a seismogram from Earth and compares it with synthetic ones for an identical source-receiver configuration on Europa, Enceladus, Titan and Ganymede to highlight the vast range of waveforms that are created by the icy-ocean environment. The paper starts with a description of the models used. In section 3, the seismic wavefield is described, a concise naming scheme is introduced and the various surface wave types in the ice layer are discussed. Section 4 applies the methodology to Europa, Titan, Ganymede and Enceladus and identifies potential seismic measurements on this representative set of icy ocean worlds.

## 2 Models and Modeling

### 2.1 Planetary models

The structural models used here were adopted from the companion paper Vance *et al.* [2017]. As described in detail there, the models include up-to-date properties for ices, saline oceans, rocky interiors and iron cores, and are thermodynamically self-consistent within the limits of available equations of state. Radial structures are computed as per Vance *et al.* (2014), with self-consistent ice and ocean thermodynamics, using boundary conditions of surface and ice-ocean interface temperature. Thermodynamics for rocks have been added as per Cammarano *et al.* [2006]. All modeling tools are freely available via GitHub (<http://github.com/vancesteven/PlanetProfile>).

Temperature profiles can be tuned to produce different ice shell thicknesses. It is also possible to consider a range of internal compositions and temperature profiles for the interior below the ocean. We consider the range of plausible ice thicknesses inferred from isostatic surface features, gravitational moment of inertia constraints, and possible radiogenic and tidal heat inputs.

For initial estimation of attenuation, we followed the approach of Cammarano *et al.* [2006] to obtain temperature and frequency dependent estimates of shear quality factor,  $Q_\mu$  with the expression

$$\frac{Q_\mu}{\omega^\gamma} = B_a \exp\left(\frac{\gamma H(P)}{RT}\right) \quad (1)$$

$$H(P) = g_a T_m, \quad (2)$$

in which  $B_a = 0.56$  is a normalization factor,  $\omega$  is the seismic frequency, exponent  $\gamma = 0.2$  is the frequency dependence of attenuation, and  $R$  is the ideal gas constant.  $H$ , the activation enthalpy, scales with the melting temperature  $T_m$  and with the anisotropy coefficient  $g_a$ , and the values of  $g_a$  chosen for various ices are described in Vance *et al.* [2017]. The bulk quality factor,  $Q_\kappa$ , is neglected.

**Table 1.** Properties of ocean worlds considered here. <sup>a</sup>*Schubert et al. [2004]* <sup>b</sup>*Thomas [2010]; Iess et al. [2014]* <sup>c</sup>*Jacobson et al. [2006]; Iess et al. [2012]*

	Radius (km)	Density (kg m <sup>-3</sup> )	Moment of Inertia
Europa <sup>a</sup>	1565.0±8.0	2989±46	0.346±0.005
Ganymede <sup>a</sup>	2631±1.7	1942.0±4.8	0.3115±0.0028
Enceladus <sup>b,c</sup>	252.1±0.2	1609±5	0.335
Titan <sup>c</sup>	2574.73±0.09	1879.8±0.004	0.3438±0.0005

It is important to note that the mineral composition and structure of the rocky interior will be very different from Earth's. For the sake of simplicity, we will use the term "mantle" for the rocky layer between water and a potential core, which may contain parts compositionally similar to terrestrial crust or even contain unknown minerals created by exotic pressure-temperature regimes. The reader can find relevant literature in the companion paper [*Vance et al., 2017*].

## 2.2 Wavefield modeling

The scope of this article is modeling the full wavefield of a layered, i.e. spherically symmetric icy world. To estimate the effect of three-dimensional heterogeneities and scattering, we introduced lateral heterogeneities into some runs. Since AxiSEM assumes an axially-symmetric model, these heterogeneities have to be symmetric around the source axis. This creates a limited scattering effect, especially since no off-path scattering is simulated, but it serves as a good first-order approximation to estimate the total effect of heterogeneities.

The reciprocity of the Green's function permits switching of the locations of source and receiver of a seismic wavefield. This has been used in the Python package *Instaseis* [*van Driel et al., 2015*], which allows to reconstruct seismograms for arbitrary source and receiver locations from a precalculated wavefield database. In models with scattering, this results in structure symmetric around the receiver axis. Theoretical arrival times, were calculated with Taup software package [*Crowell et al., 1999*] in the implementation of ObsPy 1.0 [*Krischer et al., 2015*].

Input models for all planets discussed in this article are available as an electronic supplement. The seismic wavefields are available as Instaseis databases on <http://instaseis.ethz.ch> and can be used freely for further analysis.

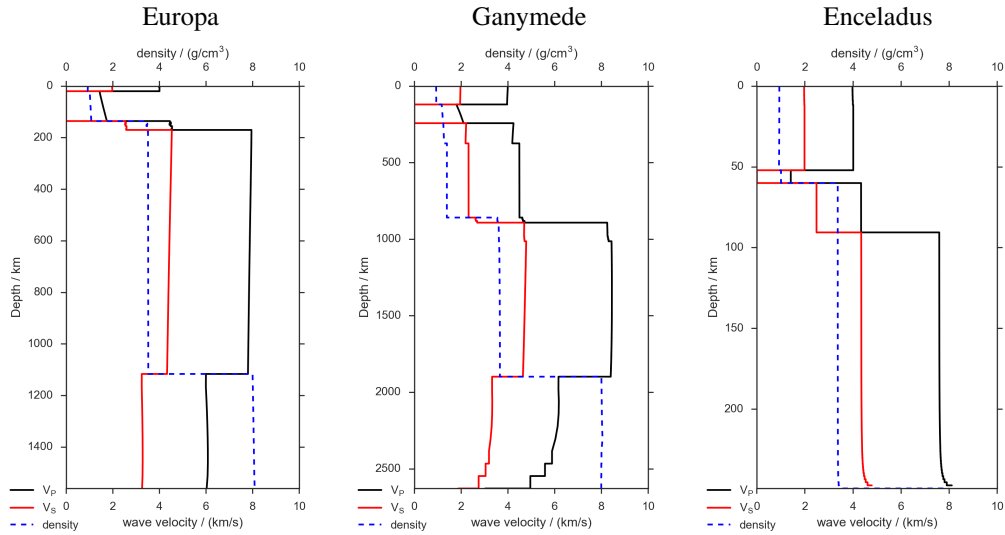


**Figure 2.** Velocity Profiles of three icy moons [Vance *et al.*, 2017]: Europa (left), with a 20km thick ice layer on top of a 116 km deep ocean with 10 weight %  $\text{MgSO}_4$ . Ganymede with (center) with a 124 km thick ice layer on top of a 116 km deep ocean and 600 km of high-pressure ice phases. Enceladus (right) has a 52 km ice layer on top of an extremely shallow ocean and no core. Compared to Earth, the velocity gradients within each layer are very small due to the relatively low density and therefore gravity. The only considerable gradients exist in the ocean.

### 3 The seismic wavefield

#### 3.1 Phase naming

##### Body waves

P	P-wave in upper ice layer or mantle
S	S-wave in upper ice layer or mantle
W	P-wave in <b>W</b> ater layer
K	P-wave in the (solid) core
E	P-wave in high-pressure ice below the ocean (German: <b>E</b> is: ice)
F	S-wave in high-pressure ice below the ocean

##### Boundaries

	<i>Surface reflections are not specifically named</i>
e	Bottom of the ice ( <b>e</b> is) layer
o	<b>O</b> cean floor
m	Top of the rocky layers ( <b>m</b> antle), if extra layers are present between ocean and mantle

##### Interface interactions

$\wedge x$	Reflection on interface $x$ from below
$\vee x$	Reflection on interface $x$ from above

##### Specific phases

Pg/Sg	P or S-waves bottoming in the uppermost ice layer
Pe/Se	P or S-waves being reflected at the ocean-ice boundary
Pn/Sn	"normal" P- or S-waves traversing all water layers, turning upwards in the mantle
Pm/Sm	P- or S-waves being reflected at the ocean/ <b>m</b> antle boundary

Prefixes for multiples. Append by integer  $N$  for multiple reverberation.  $y$  is a wildcard for any following phase.

$PwNy / SwNy$	P or S-waves being reflected $N$ times at the ocean floor and at the ocean/ice boundary; reverberation in the <b>w</b> ater
$PeNy / SeNy$	P or S-waves being reflected $N$ times at the ocean/ice boundary and at the surface; reverberation in the ice ( <b>e</b> is)

Surface waves.  $N$  is integer and indicates wave packets traveling along the minor arcs (odd numbers) or major arc (even numbers) of the great circle

CN	<b>C</b> rary wave in the ice layer
----	-------------------------------------

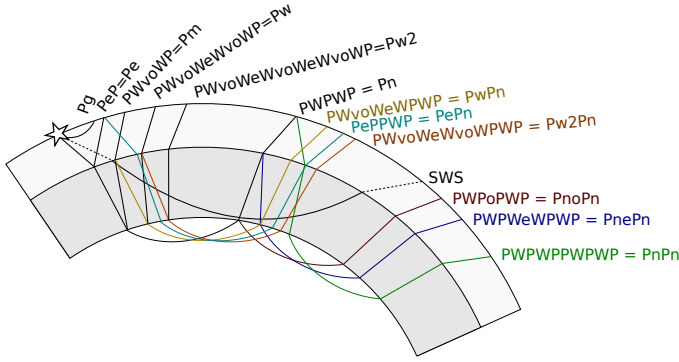


**Figure 3.** Paths of various P-phases, including multiples from the ice layer, the water layer and surface reflections for a Europa-like icy moon. Note that the thickness of the ice layer is not to scale.

To facilitate seismic analysis, it is necessary to be able to name phases (i.e. distinct signals in the seismogram) unambiguously. The terrestrial naming scheme adopted by IASPEI [Storchak *et al.*, 2003] needs to be extended in the context of icy moons to account for the various ice phases. A completely non-ambiguous scheme, which marks every interface crossing, was proposed by Knapmeyer [2003], but since it produces rather cumbersome phase names, we propose a simplified version here. Lee *et al.* [2003] proposed a scheme specifically for local waves, but since it cannot be generalized to global wave propagation, we decided do not use it here. In our scheme, all names from the IASPEI scheme keep their meaning, where applicable, but we add a few new letters for ice-specific phases. Because "i" and "I" have already been used for inner core phases, we propose "E" as the letter generally related to ice phases, using the German word "Eis" (analogous to core phases being called "K" from "Kern"). As explained before, the mantle is defined as the rocky layer between water and core and may contain minerals of the terrestrial crust and others. Path segments in the water layer are termed W. Waves in the uppermost ice layer and in the mantle are both called P or S, depending on their type. Since every receiver will be at the surface for the foreseeable future, this causes no ambiguity. A PWPWP wave is therefore one that started within the ice layer, crossed the ocean, traveled through the mantle, turned there and went back through the ocean to the surface. To retain a certain elegance in naming phases, we propose to use "Pn" for this wave type, analogous to the mantle phases on Earth as proposed by Mohorovičić [1909]. To specifically highlight local phases that never left the ice, we propose to add a "g": "Pg", "Sg", analogous to crustal phases on earth (the analogy with granite is lost here).

Interfaces will generally be called "e" for the bottom of the ice layer, "o" for the ocean floor and "m" for the top of the rocky layers, if extra ice layers are present between ocean and mantle. The IASPEI standard for marking reflections on these interfaces is not generally accepted, so we propose to stick to the intuitive TauP-convention of marking upperside reflections with "v" and lowerside reflections with "^", which can also be omitted. To keep phase names handy, we introduce a few more abbreviations: "Pe" is short for a upperside reflection from the ocean-ice interface (long: "PveP") and "Pm" is short for a upperside reflection from the mantle (long: "PWoWP"). "Pw" is a single reverberation within the water ("PWvoWeWvoWP"). These abbreviations can also be used as prefixes to mark multiples on other phases, as in "PwPn", ("PWvoWeWvoWPPWPWP"). See fig. 3 for an overview of ice- and ocean-interacting body wave paths. As on Earth, a number following one descriptor means a multiple reflection. "Pw2Pn" was reflected twice at the ocean bottom and once at the bottom of the ice layer before traveling as a P-wave through the mantle.

We show a visualization of the global wavefield in fig. 4 that follows the example of the IRIS global stack [Astiz *et al.*, 1996]. Seismograms for different distances are colorcoded,

where vertical motion is colorcoded blue, motion in R direction (towards the event) in green and transversal motion in T. Each trace is normalized separately. We see that in the coda of Pn-waves (see also fig. 5), every body wave phase is followed by multiples from the mantle-ocean and ocean-ice boundaries. See the appendix A for examples of phase names in our scheme, Knapmeyer's scheme and the popular TauP software.

### 3.2 General features of the icy-moon wavefield

#### 3.2.1 Seismic phases in the ice

Seismic events within the ice layer will create a range of seismic wave types that are not known on Earth. This is especially the case for ice layers thinner than 40 km, as suspected on Europa. The two most prominent new phases are flexural waves and the Crary phase. As shown by *Press and Ewing* [1951], the response of a floating ice layer of thickness  $d$  is similar to that of an infinite slab. *Kovach and Chyba* [2001] applied this to the situation on Europa, so that we can summarize the most important results here, assuming a compressional wave velocity  $v_{P,ice} = 4$  km/s and a shear velocity  $v_{S,ice} = 2$  km/s:

**Rayleigh waves:** Short period surface waves with vertical/radial polarization do not see the bottom of the ice layer and can therefore be described as a Rayleigh wave with the usual properties, if the inverse wavenumber  $k^{-1}$  is smaller than the ice thickness  $d$ : ( $kd = 2\pi\frac{d}{\lambda} > 1$ ).

The velocity gradient with depth is very small in the ice, so Rayleigh waves have little dispersion. For small wavelengths, the usual result of a phase velocity  $c_R = 0.92v_{S,ice} \approx 1.8$  km/s is valid.

**Rayleigh wave (ice bottom):** At short periods, an interface wave travels at the ice-water interface, called *Stoneley* wave by *Press and Ewing* [1951] and *Kovach and Chyba* [2001] (even though that term usually describes solid-solid interface waves). An interesting property is that its maximum phase velocity is controlled by the sound velocity *of the ocean*:  $c_{St} = 0.87v_{P,water} \approx 1.3$  km/s. Its signal is probably only detectable for ice shells of a few kilometers, but there, the arrival time difference with the Rayleigh wave could constrain the sound velocity of the ocean.

**Flexural waves:** Long-period vertically polarized surface waves, with  $\lambda > d$  are perturbed by the bottom of the ice layer and travel as full-layer flexural waves. The most interesting result is an intrinsic dispersion independent of the velocity structure  $c_{St} \propto f^2$ . Due to this frequency dependence, the short periods arrive first, and the group velocity of long-periods goes to zero. The cutoff frequency is where the Rayleigh regime (see above) starts.

**Love waves:** No shear waves exist in the fluid ocean, so the ice layer is a wave guide for SH waves, which are completely reflected at surface and ice-ocean interfaces. This results in a dispersive group velocity of

$$U(f) = \frac{v_{S,ice}}{\sqrt{1 - \left(\frac{nv_{S,ice}}{2fd}\right)^2}}, \quad (3)$$

where  $n = 1, 2, 3, \dots$  is the mode of the Love wave,  $v_S$ , the shear wave speed and  $d$  the ice thickness. Similar to the flexural wave, we have an inverse dispersion, where infinite frequencies travel with  $U = v_{S,ice}$ , while lower frequencies are slower. The minimum frequency of the  $n$ -th mode Love wave is

$$f_{min} = \frac{nv_{S,ice}}{2d} \approx \frac{n}{d} \text{ mHz} \quad (4)$$

for ice with  $v_{S,ice} = 2$  km/s, which is 0.2 Hz for the fundamental mode in a 5 km ice shell and 0.05 Hz for a 20 km ice shell. This minimum frequency therefore constrains the minimum ice thickness along the path.

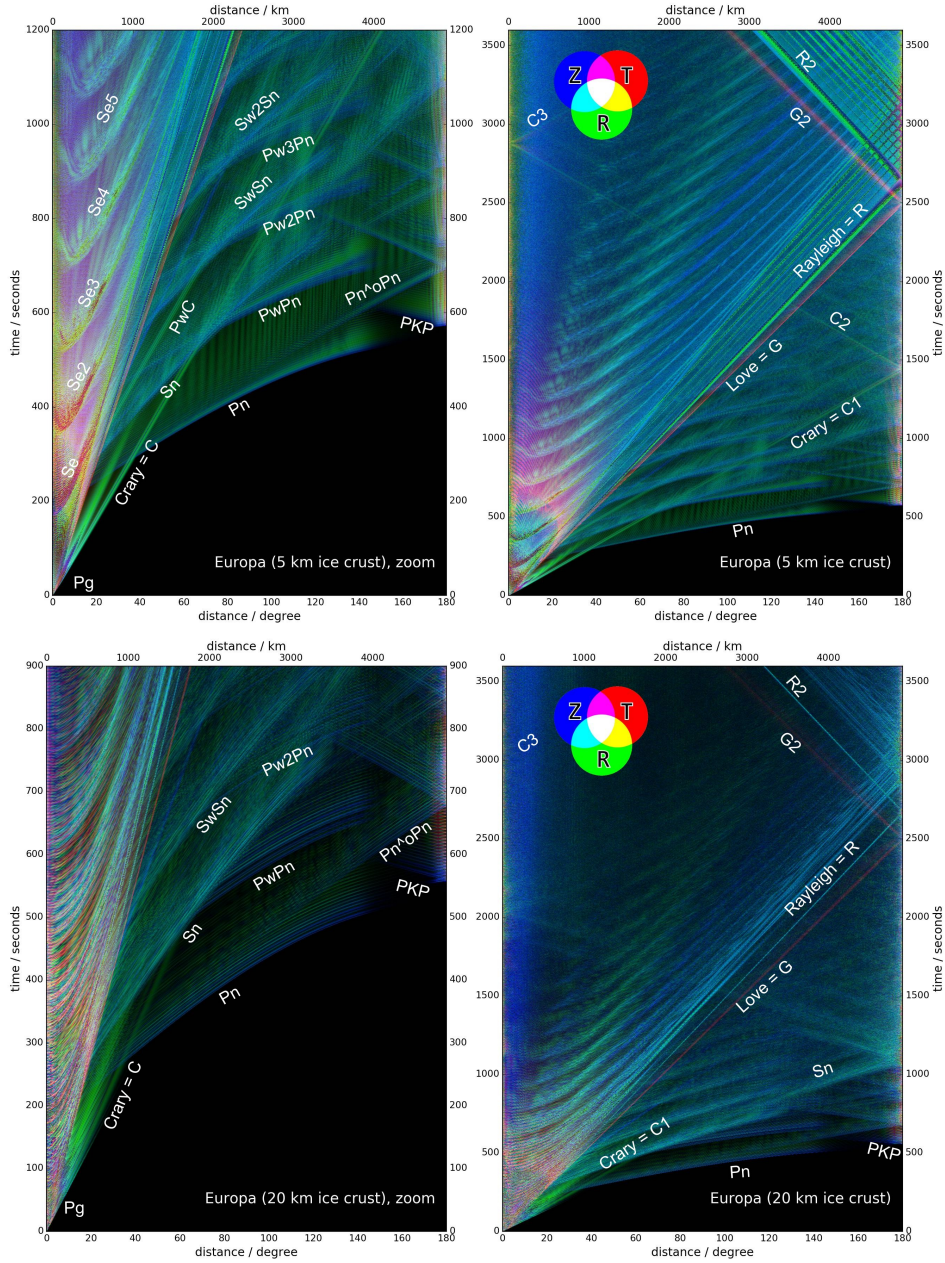


**Figure 4.** Global stack of seismograms [Astiz *et al.*, 1996] with phase names according to the scheme in table 3.1 for a Europa model with 5 km ice thickness (top) and 20 km ice thickness (bottom). C is the Crary phase in the ice, G the transversal Love wave trapped in the ice layer. Phases preceded with Pw are ocean multiples.

**Crary phase:** As a result of SV waves being completely reflected at critical angle for SV-P conversion on the boundaries of the ice, another phase arises with interesting properties [Kovach and Chyba, 2001, p. 282]: As first described by Crary [1954] with application to terrestrial floating ice in the Arctic, it has mainly radial displacement, a phase velocity of  $v_P$  (for homogeneous ice layers) and a characteristic frequency of

$$f_{Cr} = \frac{v_S}{d\sqrt{1 - \left(\frac{v_S}{v_P}\right)^2}}. \quad (5)$$

Measurement of  $f_{Cr}$  constrains the ice thickness  $d$ , assuming  $v_S$  and  $v_P$  are known to a reasonable extent. Since  $f_{Cr}(d = 5\text{km}) = 0.46\text{ Hz}$  and  $f_{Cr}(d = 20\text{km}) = 0.11\text{ Hz}$ , the thickness of Europa's ice layer can be easily measured with a seismometer that is sensitive at these frequencies. Compared to other surface waves, the Crary phase has a high phase velocity, which means that it arrives much before all other ice phases at long distances, and even before mantle body waves at intermediate distances (see tab. 3.2.4). For ice thicknesses above 40 km, the maximum frequency becomes too low to be observable for realistic events with a space-ready seismometer.

Especially for thin ice layers, the wavefield has two frequency regimes: Most of the phases specifically related to the ice layer (Crary phase, flexural waves) have a maximum frequency between 0.1 and 0.5 Hz (for thicknesses of 20 and 5 km resp.), depending on ice thickness. Body waves from the mantle are not limited in maximum frequency and should thus be clearly distinguishable. Scattering within the ice layer enhances this effect by damping high frequency ice body waves, with paths in the ice layer.

Due to the negative velocity jump at the ice-ocean boundary, ray paths are bent towards the normal. This means that wave energy refracted into the ocean will mostly not return to the ice layer until it has been reflected at the ocean floor. Diffracted waves exist, similar to Pdiff at the core-mantle boundary on earth, but generally ice-body waves fade away after a short distance.

### 3.2.2 Water phases

Due to the large velocity contrast between compressional wave velocity in the ice and in the water, no phases like PWP exist in shallow ocean worlds like Europa, while they would be a dominant signal in the late seismogram on Ganymede, Titan and possibly Enceladus, depending on the ice thickness of the latter.

Attenuation in water is very small, so phases that are multiply reflected at the top and bottom of the ice layer are observable almost over the whole distance range. Their polarization is mainly on the radial component.

### 3.2.3 Mantle phases

Mantle body waves cover the whole frequency range. On Europa, they dominate the seismic signal above 0.2 Hz. The effect is, that a broadband seismometer, sensitive enough to measure in the whole frequency range can estimate the wave type from its frequency content alone. It also means that while displacement amplitudes are dominated by ice phases after their arrival, body waves might still be recovered from the high-frequency content of the seismogram.

The Scholte wave is one particular mantle phase occurring at the ocean bottom. This wave shares most characteristics of a Rayleigh wave, but is defined on a solid-fluid interface [Scholte, 1947]. Its phase velocity is frequency-dependent, but below the shear velocity in the solid and the sound velocity in the fluid, whatever is lower [Rauch, 1980], i.e. below 1.8 km/s. It has been used in marine exploration on Earth to estimate the shear wave velocity of the uppermost layers below the seafloor [Nolet and Dorman, 1996; Kugler et al., 2005]. If

it can be detected, a detailed dispersion analysis might be used to constrain the existence of hydrated low-velocity layers on the sea floor. As it can be seen in Figure 4, it shows strong water multiples.

### 3.2.4 Distance regimes

In terrestrial seismology, several distance regimes are defined, because seismograms change their first order shape considerably from one to the next [Kennett, 2002]:

**Local (0 to 100 km)** For shallow events, the ground displacement is controlled by the near field of the source and significant permanent deformation occurs at the surface. The local regime can be considerably larger for mega-thrust events [Grapenthin and Freymueller, 2011].

**Regional (100–1000 km)** Crustal body wave phases arrive first. Crustal S-waves and surface waves form one wave train (Lg).

**Far regional (1000–3000 km)** Mantle body wave phases arrive first and are separated from the surface wave train, but due to the upper mantle discontinuities, multiple (triplicated) phases arrive within a short time window.

**Teleseismic (3000–9000 km)** Mantle body wave phases are clearly separated from each other and are visible in the seismogram as well-defined sharp pulses. Direct body waves do not sense the core yet.

**Core shadow (beyond 9000 km)** Direct P-waves are shadowed by the core and multiple complex core phases arrive first, followed by surface-reflections (PP).

To summarize, the distance regimes define whether the first arriving phases have mainly travelled through the crust, the complex upper mantle, the homogeneous lower mantle or the core. The situation on icy ocean worlds is similar. We propose to separate the following regimes:

**Local** Near field effects are dominant, including permanent displacement.

**Regional** Body waves that traveled through the ice layer only arrive first.

**Ocean shadow** Direct body waves are masked by the curvature of the planet’s surface. The first- arriving phases are Crary waves and Love waves.

**Teleseismic range** Mantle body waves arrive first

**Core shadow** The planetary body’s core masks direct body waves.

The distance range of these regimes depends mostly on the thickness of the ice layer. An exception is the local regime, whose size depends mainly on the magnitude of the event, but also highly on the local velocity structure. On thin-ice worlds like Europa, considerable coseismic displacement will occur over hundreds of kilometers, but its long periods will not be detectable with a space-ready seismometer. Therefore, we do not discuss this region in detail here.

The distance regimes for a set of icy ocean worlds can be found in table 3.2.4. For the thin-ice worlds like Europa, it is very unlikely that an event will randomly fall into the regional area around a lander, where direct ice phases are well-recordable. Roughly 5% of randomly distributed events will be in the ocean shadow range, where special ice layer phases will be the first arrivals. The remaining more than 90% of events will be beyond that in the range, where mantle and core body waves arrive first.

## 3.3 Single-station seismology on icy moons

The first efforts of seismology on icy moons will probably be conducted from a single station. Single-station seismology was the default on Earth for decades and all the fundamental discoveries, like the Mohorovicic discontinuity or the outer and inner core were de-

Moon		regional	ocean shadow	teleseismic
Europa	5 km ice	0 – 5° (0.2%)	5 – 30° (6.5%)	30 – 150° (86.6%)
Titan	33 km ice	0 – 20° (3%)	20 – 55° (18.3%)	55 – 160° (75.7%)
	114 km ice	0 – 50° (17.9%)	- (0%)	50 – 150° (75.4%)
Ganymede		0 – 60° (25%)	- (0%)	60 – 120° (50%)
Enceladus			5 – 80° (41.1%)	80 – 180° (58.7%)
Earth		1 – 10° (0.75%)	10 – 30° (5.9%)	30 – 105° (56.4%)

**Table 2.** Distance ranges of seismograms regimes on different icy worlds. Epicentral distances between earthquake and receiver are noted in degrees. The number in parentheses notes the fraction of the total planetary surface that is covered by this distance regime. If we assume a random distribution of events on the surface, this is also the probability that any given event will fall into this distance range from a lander. For comparison, the distance ranges on Earth are also noted, where "ocean shadow" corresponds to "regional earthquakes".

rived from observations of earthquakes on single observatories [Oldham, 1906; Mohorovičić, 1909; Lehmann, 1936]. It has long been shown that parameters of earthquakes can be determined from one station alone [Ekström *et al.*, 1986; Wu *et al.*, 2006]. A large body of work on single-station seismology has been done in the context of the Mars seismometer on the InSight lander [Panning *et al.*, 2015; Khan *et al.*, 2016; Böse *et al.*, 2016]. Here, the location of an earthquake is determined by the polarisation of P and surface waves and the time difference between specific phases.

Since the Crary wave is a prominent feature in the seismogram of Europa, it can be used for fast determination of the backazimuth of the event (the direction as seen from the seismometer). Its energy loss due to attenuation is relatively low, so it propagates around the planet multiple times. From the time difference between these orbits, the distance can be determined. On thick-ice worlds, the Rayleigh wave can take this role. Smaller local events can be located using the time difference between Pg and Sg phases, as well as reflections from the ice-ocean boundary (PeS or PeP), once the ice thickness has been constrained. This constraint is best achieved using distant events, using the following work flow:

1. Estimate the ice thickness from converted waves in the coda of body waves of distant events. This analysis needs no event localization and not even a clear identification of phases (see fig. 5). The coda contains clearly recognizable multiples, whose time difference is the ice thickness divided by the wave velocity.
2. With the constraint from step 1, refine the thickness estimate from the cutoff frequency of the Crary wave (for ice layers < 40 km) and estimate P- and S-wave velocities in the ice.
3. With an ice layer model, locate local events.
4. From multiple-orbit Crary or Rayleigh waves, locate distant events.
5. Identify ocean multiples in the coda of body waves of distant events and constrain the ocean depth (see Fig. 5).
6. If direct ocean phases (PWP, SWS) have been identified together with body waves, the speed of sound in the ocean can be estimated, constraining the ocean chemistry.
7. Identify Scholte waves at the ocean bottom to constrain the uppermost mantle structure below the sea floor from dispersion curves (see Fig. 8).
8. Identify as many body wave arrivals as possible to constrain mantle velocity structure with the event locations from step 4.

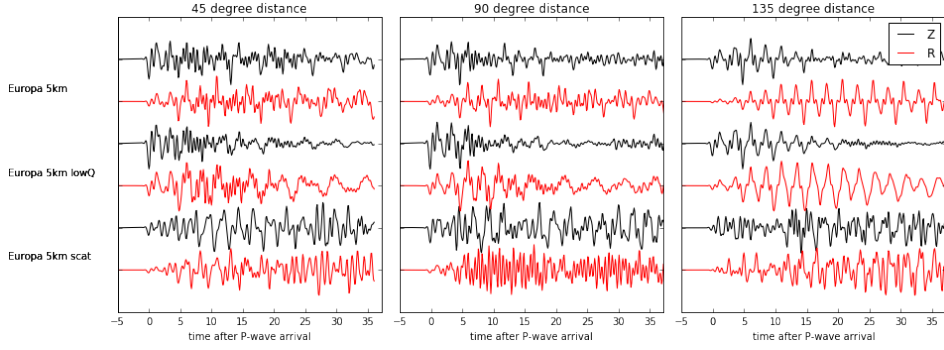


**Figure 5.** Coda of a Pn wave measured at 45, 90 and 135 degree distances for various Europa models. Black lines correspond to vertical displacement (Z-component), red to horizontal pointing away from the source (R-component). Clearly visible are the reverberations from the ice layer, which will serve to estimate the ice thickness from a single seismogram. The effect is clearest for very large distances (135 degree), where the incident angle is almost vertical. The horizontal component seismograms have their maximum energy several seconds after the vertical seismogram. The lowermost models have been modified to simulate the effect of a highly attenuative ice layer (lowQ) or of a low-attenuation, high-scattering model, similar to the lunar crust (scat). Here, the reverberations become much less pronounced, but are still visible, especially on the long-distance horizontal components. Note that 45 degree seismograms contain triplicated phases, which creates the very complex waveform.

**Table 3.** Overview of some of the icy ocean worlds of the solar system

name	radius [km]	ice thickness	ocean depth	high-P ice layers?	
Europa	1561	5–30 km	>100 km	no	
Ganymede	2631	>50 km	>100 km	yes	[Vance <i>et al.</i> , 2014]
Enceladus	252	10–50 km	40 km	no	[Vance <i>et al.</i> , 2017]
Titan	2575	33–146 km	80 km	maybe	[Vance <i>et al.</i> , 2017]

## 4 Icy ocean worlds in the solar system

### 4.1 Europa

Europa has been the subject of the most detailed studies to date and a lander mission could take place in the coming decades [Hand *et al.*, 2017]. Therefore, we discuss wave propagation and measurability of seismic waves in detail here.

#### 4.1.1 Overview

Compared its radius, Europa has a thinner ice layer than all all other icy ocean worlds. This creates pronounced ice-layer specific seismic phases. The transition from a ice-Rayleigh wave to flexural waves occurs between 0.1 Hz (for 20 km ice thickness) and 0.5 Hz (for 5 km ice), which would be well observable with a wide-band seismometer, as the SP instrument used for InSight [Pike *et al.*, 2016] and proposed for the NASA Europa lander.

In a ray-geometrical setting, no PWP-phase exists, that turns in the water column. The ray parameter of a horizontal wave at the bottom of the ocean would be  $p = 14.1 \text{ s/deg}$ , which is higher than the maximum ray parameter at the surface of  $p = 6.85 \text{ s/deg}$  for P-waves in the ice and  $13.86 \text{ s/deg}$  for S-waves. Since the slowness gap for SWS is sufficiently low, SWS is possible at longer periods and creates a pronounced signal at distances up to 60 degree. A peculiar point is that in a salty ocean with 10%  $\text{MgSO}_4$  and a 10% higher sound

speed [Vance *et al.*, 2017] the ray parameter of a SWS wave would be just  $p = 12.98\text{s/deg}$ , so that SWS would have a strong signal within a certain distance range, creating a seismic observable to constrain the ocean chemistry.

Due to its modest size, multiple planetary orbits of seismic ice-phases, especially the Crary wave should be observable with the SP instrument, which would allow for a straightforward inversion for the distance of a seismic event. Due to the thin ice layer, no SH waves are possible beyond 100 km, so that the transversal component will be very distinct from the radial component, allowing an estimation of the event backazimuth.

In a companion paper [Panning *et al.*, 2017], we estimate the background seismicity from tidal cracking and show that it should be detectable with a seismometer. This seismicity will create a significant seismic hum, that can be used for ambient noise analysis techniques, to constrain the thickness of the ice layer or mantle discontinuities.

#### 4.1.2 Measurability

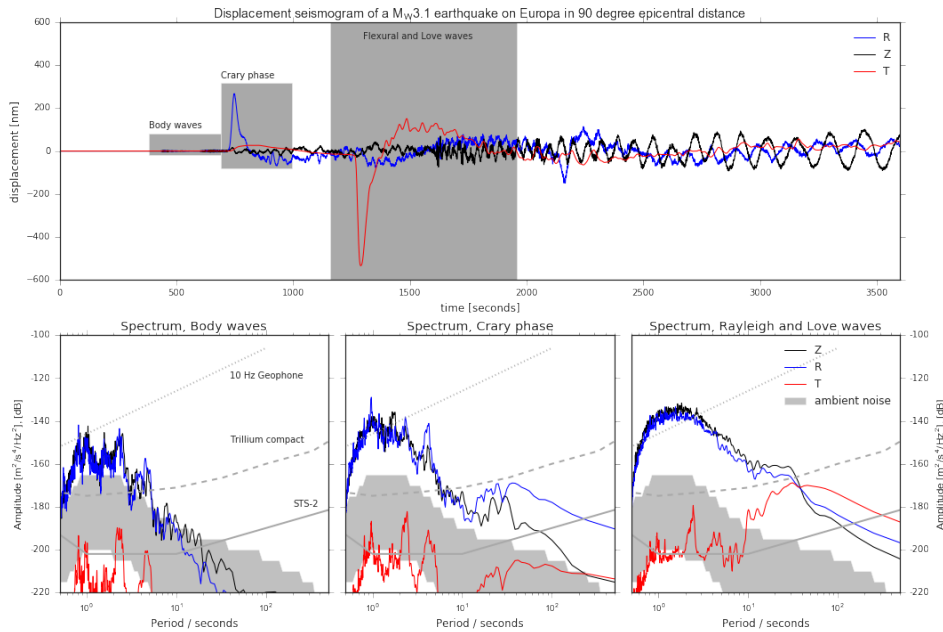


**Figure 6.** Measurability of seismic phases on Europa: The upper plot shows an exemplaric seismogram of a  $M_W = 3.1$  earthquake in 2 km depth in the ice shell in 90 degree distance. The velocity model has a 5 km thick ice layer, with high  $Q$  (low attenuation) and strong scattering (Karman medium, 5 km correlation length, amplitude 10%). Three significant time windows are selected: A) a body wave window between 380 and 690 seconds, which contains only waves that travelled through the mantle. B) a window with the Crary wave, a nondispersive wave within the ice layer that consists of pure vertical partial motion and C) a window in the later seismogram, where surface-wave-like phases arrive on all components. The lower plots show spectra of these three time windows vs established self-noise models of typical instruments, based on Ringler and Hutt [2010]. To account for effects of radiation pattern and source depth, the spectra are averages of 100 events with depths between 0 and 5 km and random focal mechanisms. The grey area in the spectra corresponds to the 1st and 9th decile of the noise model C in Panning *et al.* [2017], simulating seismic noise due to tidal cracking.

**Table 4.** Titan model used for detectability test of an IceVI layer as shown in fig. 8

Layer	thickness [km]	$v_P$ [km/s]	$v_S$ [km/s]	$\rho$ [kg/m <sup>3</sup> ]
Iceh	46	3.9	2	925
ocean	410	1.55 – 2.55	–	1020 – 1170
IceVI	5.5	4.4	2.26	1394
mantle		7.99	4.54	3526

Any realistic lander mission on an icy world will face severe constraints in terms of seismometer mass: in the Report of the Europa lander Science Definition Team [*Hand et al.*, 2017], the baseline instrument was defined as equal to the Short Period (SP) instrument of the InSight Mars lander. Its self-noise level in an Europa environment will be probably close to that of a Trillium compact seismometer on Earth. We therefore tested, which seismic phases could be detected with such an instrument for a magnitude 3.3 earthquake at a distance of 90 degree (fig. 6). Body waves exceed the instrument self-noise by 20 dB between 0.1 and 2 Hz and will therefore be well observable. The Crary phase, which is crucial for event location, exceeds the self-noise by 30 dB. The late seismogram on R and Z, including Rayleigh and flexural waves can be measured for periods up to 50s. The Love wave on T, which is confined to the ice layer and therefore strongly affected by attenuation and scattering in the ice, is not observable for most focal mechanisms. Based on the seismicity model in *Panning et al.* [2017], that is based on a Gutenberg-Richter magnitude distribution, analogous to the one proposed by *Golombek et al.* [1992] for Mars, a magnitude 3.3 event can be expected to occur somewhere between once a week and once a month.

## 4.2 Titan

Titan is predicted to have water and ice layers of around 480 km above a silicate mantle. The ice covering is interpreted to be 55-80 km based on the observed Schumann resonance [*Béghin et al.*, 2012]. Following *Vance et al.* [2017], we consider thicknesses in a slightly wider range between 33 and 124 km. Depending on the ocean’s temperature profile with depth, high-pressure ice phases might be present below the ocean with a total thickness of up to 230 km or not present at all. Depending on the ocean temperature, the ice thickness may be so high that the Crary and flexural waves are restricted to long periods, unobservable with the a realistic instrument. Because the rocky mantle makes up more than 80 % of the diameter in all models, the teleseismic range dominates on Titan (see fig. 7).

An important question for habitability in Titan is the existence of high-pressure ice phases at the bottom of the ocean. If they are present, they may form a barrier to water-rock interactions that regulate redox and ocean composition, and which are thereby critical for supporting life. While intra-ice convection might be able to transfer ions [*Choblet et al.*, 2017], the absence of a high-pressure ice layer would benefit habitability. Because such a layer is not detectable with radar or moment-of-inertia measurements, seismological measurements provide an unique opportunity. As it was argued in *Vance et al.* [2017], the thickness of surface ice above the ocean and high-pressure ice below are strongly correlated and both mainly controlled by the ocean ion content and temperature profile. According to these simulations, every model with a surface ice thickness of more than 50 km must also contain high pressure ice layers. Seismic methods could constrain surface ice and high pressure ice thicknesses independently and thereby constrain ocean chemistry and temperature.

As one example, Figure 8 shows a comparison of waveforms for two thin surface ice models (47 km) on top of a 410 km deep ocean with 3.3 weight percent NH<sub>3</sub> (similar to the 3 wt percent NH<sub>3</sub> model with 265 K in table 7 of [*Vance et al.*, 2017]). For this surface ice thickness, high pressure ice can neither be confirmed nor excluded. The figure compares seismograms of this model with one where the IceVI layer has been replaced by mantle

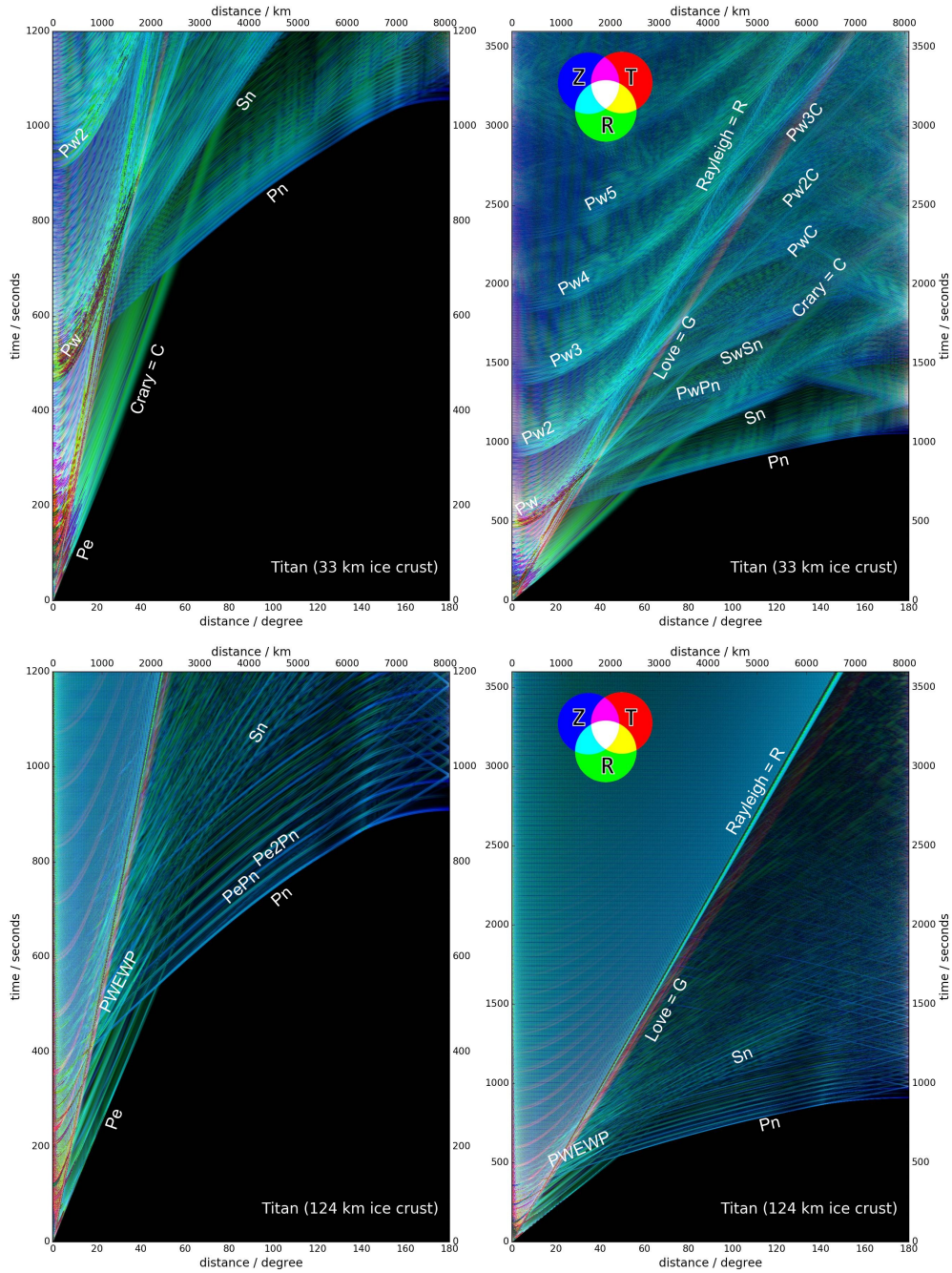


**Figure 7.** Global stack of seismograms for a Titan model of 33 km ice thickness (pure water ocean and 270K in table 7 of Vance *et al.* [2017], top, compared to one with 124 km ice (bottom, model with 3% $\text{NH}_3$  ocean and 255K in table 7 of Vance *et al.* [2017]). The thinner ice model has a seismic wavefield resembling that of Europa, with a dominant Crary phase that is the first arriving phase between 20 and 55 degrees. In the thick-ice model, special ice phases (esp. the Crary wave) are negligible and the wavefield is more similar to a terrestrial planet, where body waves always arrive first. In difference to Earth or Mars, every phase is followed by a large number of multiples from ice and/or the ocean.

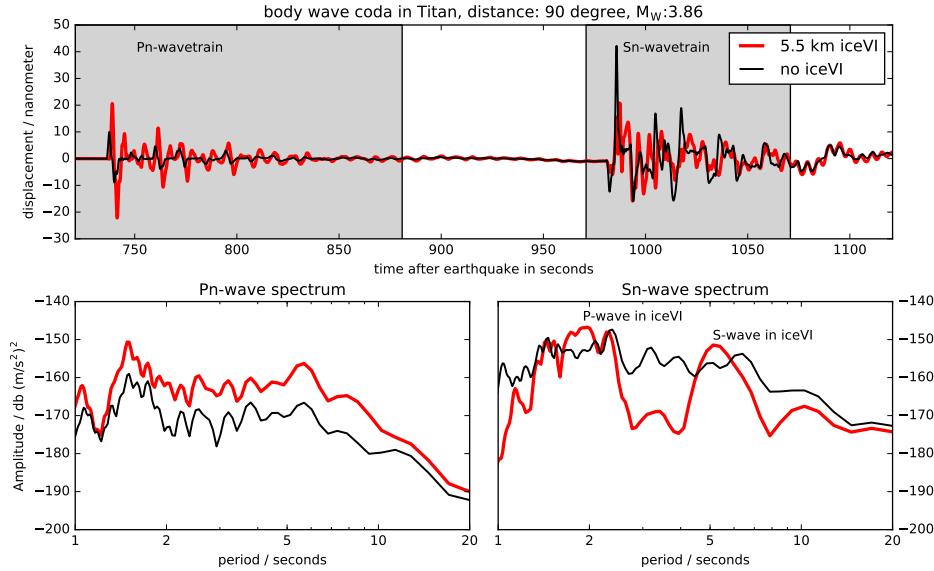


**Figure 8.** Detectability of an high-pressure ice layer (IceVI) below the ocean from body and Scholte waves. The upper plot shows the vertical displacement of an M3.8 earthquake in 90 degree distance and 5 km thickness for two interior models with 33 km ice thickness. The red lines correspond to a model with a 5.5 km IceVI layer the bottom of the ocean. The model displayed with black lines is identical, but the mantle starts directly below the ocean. The lower two plots show acceleration spectra of a window around the P-wave arrival (left grey patch in upper subfigure) and the S-wave arrival (right grey patch in upper subfigure). The amplitude of the Pn wave train in a model with an ice layer is two times higher than in the model without the layer. Since it will be difficult to reliably determine the magnitude of an earthquake with just one station, this effect may go unnoticed. The spectrum of the S-waves (lower right) however, shows clear effects of the IceVI layer: While the spectrum of the simple model is almost flat between 1 and 10 seconds, the IceVI layer produces two clear peaks at 2 and 5.1 seconds, corresponding to reverberations of P and SV waves. This signal should be easily distinguishable, even without a detailed source model.

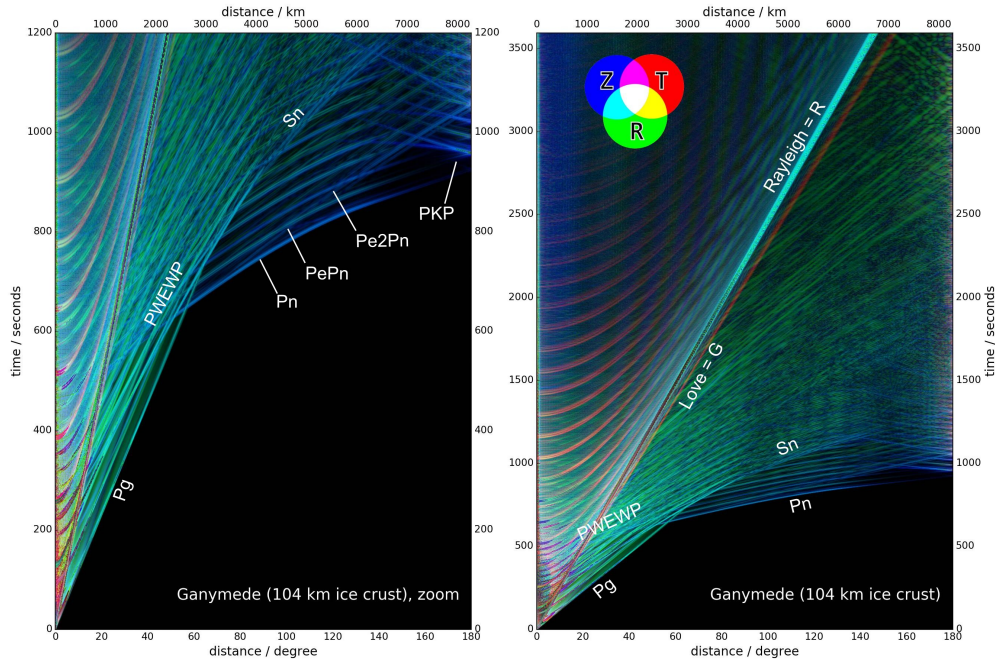


**Figure 9.** Global stack of seismograms for a Ganymede model of 104 km ice thickness. The thick ice layer creates nicely separated body wave reverberations in the ice. Seismic waves that bottomed in the high pressure ice layer (PWEWP) arrive in the coda between 20 and 90 degree distance. They seem to connect to Sn at 90 degree, since the P-velocity in the high-pressure ice is very close to the S-velocity in the mantle. The overall wavefield is very similar to a cold-ocean Titan.

(see table 4). Because there is no distance where high-pressure ice phases arrive first, their presence will have to be inferred from the coda of mantle body waves. The strong velocity and density increase at the ocean-mantle interface (assuming that no iceVI layer is present) causes a strong impedance contrast, which is weakened, if there is an intermediating layer.

Titan is the only icy ocean world with an atmosphere. Due to the atmosphere's low density, the direct effect on the seismic wave propagation in the planet will be minimal, however, it could serve as a source for seismic signals: Wind waves on Titan's methane lakes have been predicted to reach significant wave heights of 0.2 m at periods of 4 seconds [Lorenz and Hayes, 2012], even though this could not be confirmed yet by Cassini measurements [Hofgartner et al., 2014; Zebker et al., 2014]. If such waves existed, they would create pressure on the sea floor of the order of 100 Pa, which is comparable to pressure variations on the abyssal sea floor on Earth due to surface wave interference [Cox et al., 1984]. Because the latter creates a globally observable seismic signal [Kedar et al., 2008], it must be assumed that measurable ocean-generated microseisms are possible on Titan. Surface waves from this signals could be used to constrain the uppermost layers below the surface.

Pressure changes in the atmosphere might also create seismic signals directly, as it is observed for long periods on Earth [Peterson, 1993; Beauduin et al., 1996] or local phenomena, such as "dust devils" on Earth and potentially Mars [Lorenz et al., 2015]. Conversely, seismic waves will create atmospheric signals, that might be detectable from orbit, as observed on Earth and proposed for Venus [Lognonné et al., 2016].

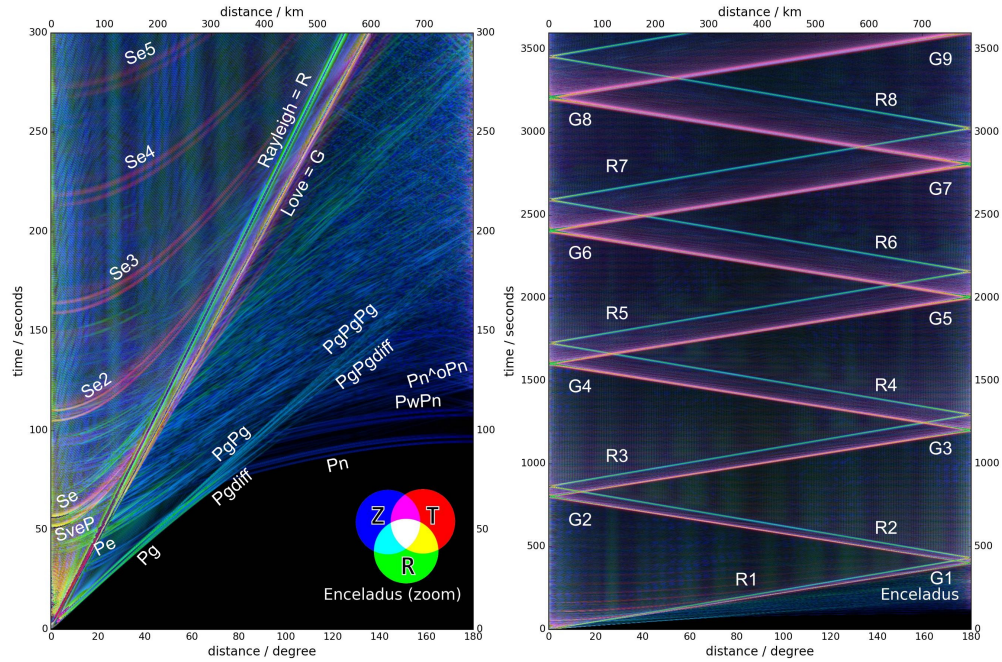


**Figure 10.** Global stack of seismograms for a Enceladus model of 52 km ice thickness. Since this is 20% of the radius, ice phases (Pg, Pgdiff) are the first to arrive up to 75 degree distance and surface reflected ice phases (PpPg, PpPpPg) are prominent in the coda for all distances). The ice layer is too thick for a measurable Crary phase the ocean below the ice is only 10 km deep. Due to the small diameter and the relatively low attenuation, surface waves orbit the moon multiple times and dominate the seismogram (see fig. 1).

### 4.3 Ganymede

The density structure inferred from moment of inertia measurements suggests that Ganymede has water layers in different forms of 800 km above a rocky mantle and an iron core [Vance *et al.*, 2014]. The uppermost ice layer is assumed to have a thickness of more than 50 km, followed by a liquid ocean of more than 100 km depth. Due to the high gravity and abundance of water, pressure at the ocean floor creates layers of ice V and VI between the liquid ocean and the rocky mantle. Similar to Titan, the existence and thickness of these layers can only be constrained by seismology. Since both are controlled by ocean chemistry and temperature, this creates a direct geophysical observable for habitability conditions of the ocean.

The thick ice layer means that Crary phases are relatively weak and constrained to long periods, which makes them unobservable without a true high-sensitivity broadband seismometer. The ice thickness therefore would have to be constrained from multiples in the coda of body waves. Compared to Titan, the thickness of the combined water layers is 30% higher, which clears the coda of body waves.

### 4.4 Enceladus

Enceladus' global subsurface ocean has been confirmed from its measured shape [McKinnon, 2015] and libration [Thomas *et al.*, 2016], but its depth probably varies globally, with a depth of more than 15 km at the south pole and less than 10 km elsewhere. For the simulation, we assumed a constant depth of 10 km everywhere.

Due to its small size, geometrical spreading and attenuation of seismic energy plays a small role on Enceladus. Even for magnitude 3 events, more than 5 orbits of Crary phases are observable, which would allow for an easy determination of ice thickness and event locations. Tidal heating from the resonance with Dione suggests a high energy budget for seismicity, consistent with the active tectonic deformation of the South Pole region [Porco *et al.*, 2006]. This high seismicity would create a high seismic background noise that could be harnessed using ambient noise techniques. On Enceladus, it might be possible at much shorter periods.

## 5 Discussion

This study gives an overview over general characteristics of icy moon seismology on a global scale, but is in no way exhaustive. An obvious limitation is that only spherical models were studied so far. The above-mentioned methods to determine the ice thickness are sensitive ice undulations. The maximum frequency of the Crary wave is sensitive to the average thickness. The Love wave cutoff is sensitive to the minimum thickness, while body wave coda measures the thickness at the location of the source and the receiver. Enceladus for example has an ellipticity of 1/50, and probably a variation in ice and ocean thickness of more than 50% between the south pole and the equator [Thomas *et al.*, 2016], which will strongly affect propagation, especially of multiply orbiting surface waves. From simulations using cylindrically symmetric models, we found that the Crary wave is a very robust feature and multiple orbits are detectable, even with strong heterogeneities in the ice. Nevertheless, undulations of the ice bottom may have a very strong effect on the dominant frequency of the Crary wave and therefore on its effectiveness in constraining ice thickness.

On Europa and Enceladus, the existence of plumes suggests that liquid channels exist in the ice that will strongly scatter seismic waves. Therefore, full-3D simulations will be necessary as a next step.

Seismic wave propagation on icy ocean worlds is a numerically challenging problem, since it requires high frequencies of up to one Hertz to resolve seismic features like the Crary wave for thin ice layers. Since numerical cost in full 3D methods typically scales with frequency  $f$  as  $O(f^4)$ , this prohibits their application on planet scales. At the same time, the ice waves may be very sensitive to three-dimensional structure, like varying ice thickness. This is rather different from the situation on Earth, where surface waves are strongest at longer periods (typically above 15 seconds), which are possible to simulate on large HPC systems. Seismic wavefield solvers for three-dimensional structure on planetary scale at frequencies of up to one Hertz are just becoming available [Leng *et al.*, 2016] and will offer more insight into the question which phases are usable. Local structure around a lander may strongly affect the measured seismic waveforms, which may be simulated by including local 3D wavefield simulations into global 1D simulations.

This article is intended to set the stage of global seismic wave propagation in icy moons on which more detailed studies of effects of three-dimensional structure can build.

Since the presented analysis of the seismic wavefields is in all likelihood incomplete, we make the Instaseis databases available at <http://instaseis.ethz.ch>. The scripts to reproduce the figures are available on the seismo-live website <https://www.seismo-live.org>.

Future research should also explore the parameter space of possible mantle compositions and thermal states. As it was shown here, seismology in principle provides tools to constrain both, but detailed studies are necessary for each planetary body in close collaboration with planetary geophysics.

Scientific objective	Seismic observable	signal strength	distance range
Ice thickness	Resonant frequency of Cray phase	strong signal	global
	Transition frequency between Rayleigh and flexural surface wave	intermediate	global
	Reverberations in body wave coda	strong	teleseismic
	Autocorrelation of noise	strong	does not require single events
Ocean depth	Reverberations in body wave coda	strong	teleseismic
	Autocorrelation of noise	strong	does not require single events
	existence of SWS/PWP	strong	20 to 70 degree distance
Ocean chemistry (from sound velocity in water)	Reverberations in body wave coda	strong	teleseismic
	existence of SWS/PWP	strong	20 to 70 degree distance
High pressure ice phases	Coda of Sn/Se-waves	strong	teleseismic
	Scholte waves P-to S ratio	strong intermediate	teleseismic teleseismic, depends on focal mechanism
Core diameter	Autocorrelation of noise	weak	ambient noise
	Autocorrelation of seismogram	intermediate	> 100 deg

**Table 5.** Potential scientific objectives of a future icy ocean world seismometer and seismic observables that address it.

## 6 Conclusion

In this paper, we discussed the general characteristics of global seismology on icy ocean worlds. The existence of the liquid-filled gap between the mantle and the icy crust creates a different wavefield than the one that is known on earth. In general, this means that a large part of seismic energy remains close to the surface, where it can be measured, which makes even relatively small events observable globally. Also, several seismic measurables are specifically sensitive to parameters related to habitability. This is a promising perspective for the short term installations of seismometers currently envisioned by NASA.

## Acknowledgments

The authors acknowledge computational support in the project pr63qo "3D wave propagation and rupture: forward and inverse problem" at *Leibniz-Rechenzentrum* Garching. SCS was supported by grant SI1538/4-1 of Deutsche Forschungsgemeinschaft *DFG*. MvD was supported by grants from the Swiss National Science Foundation (SNF-ANR project 157133 "Seismology on Mars") and the Swiss National Supercomputing Center (CSCS) under project ID sm682.

This work was partially supported by strategic research and technology funds from the Jet Propulsion Laboratory, Caltech, and by the Icy Worlds node of NASA's Astrobiology Institute (13-13NAI7\_2-0024). A part of the research was carried out at the Jet Propulsion Laboratory, California Institute of Technology, under a contract with the National Aeronautics and Space Administration.

The Instaseis wavefield databases available at <http://instaseis.ethz.ch>. The scripts to reproduce the figures are available on the seismo-live website <https://www.seismo-live.org>.

All rights reserved prior to publication.

**A: Phase names compared with other naming schemes**

Our scheme (short)	our scheme (full)	Knapmeyer	TauP
Pn	PWPWP	POPoPopOp	P20P136P136P20P
Pg	P	P	P
PWP	PWP	POPOP	P20P20P
PnPn	PWPWPPWPWP	POPoPopOpPOPoPopOp	P136PP136P

**References**

- Astiz, L., P. Earle, and P. M. Shearer (1996), Global Stacking of Broadband Seismograms, *Seismological Research Letters*, 67(4), 8–18, doi:10.1785/gssrl.67.4.8.
- Beauduin, R., P. Lognonné, J. P. Montagner, S. Cacho, J. F. Karczewski, and M. Morand (1996), The effects of the atmospheric pressure changes on seismic signals or how to improve the quality of a station, *Bulletin of the Seismological Society of America*, 86(6), 1760–1769.
- Béghin, C., O. Randriamboarison, M. Hamelin, E. Karkoschka, C. Sotin, R. C. Whitten, J. J. Berthelier, R. Grard, and F. Simes (2012), Analytic theory of Titan’s Schumann resonance: Constraints on ionospheric conductivity and buried water ocean, *Icarus*, 218(2), 1028–1042, doi:10.1016/j.icarus.2012.02.005.
- Böse, M., J. Clinton, S. Ceylan, F. Euchner, M. van Driel, A. Khan, D. Giardini, P. Lognonné, and W. Banerdt (2016), A Probabilistic Framework for Single-Station Location of Seismicity on Earth and Mars, *Physics of the Earth and Planetary Interiors*, 262, 48–65, doi:10.1016/j.pepi.2016.11.003.
- Bruzzzone, L., J. Plaut, G. Alberti, D. Blankenship, F. Bovolo, B. Campbell, A. Ferro, Y. Gim, W. Kofman, G. Komatsu, W. McKinnon, G. Mitri, R. Orosei, G. Patterson, D. Plettemeier, and R. Seu (2013), RIME: Radar for Icy Moon Exploration, in *2013 IEEE International Geoscience and Remote Sensing Symposium - IGARSS*, pp. 3907–3910, IEEE, doi:10.1109/IGARSS.2013.6723686.
- Cammarano, F., V. Lekic, M. Manga, M. P. Panning, and B. Romanowicz (2006), Long-period seismology on Europa: 1. Physically consistent interior models, *Journal of Geophysical Research*, 111(E12), E12,009, doi:10.1029/2006JE002710.
- Cassen, P. S., J. Peale, and R. T. Reynolds (1979), Is there liquid water on Europa?, *Geophysical Research Letters*, 6, 731–734.
- Choblet, G., G. Tobie, C. Sotin, K. Kalousová, and O. Grasset (2017), Heat transport in the high-pressure ice mantle of large icy moons and the dissipation number, *Icarus*, 285, 252–262, doi:10.1016/j.icarus.2016.12.002.
- Cox, C., T. Deaton, and S. Webb (1984), A Deep-Sea Differential Pressure Gauge, *Journal of Atmospheric and Oceanic Technology*, 1(3), 237–246, doi:10.1175/1520-0426(1984)001<0237:ADSDPG>2.0.CO;2.
- Crary, A. P. (1954), Seismic studies on Fletcher’s Ice Island, T-3, *Transactions, American Geophysical Union*, 35(2), 293, doi:10.1029/TR035i002p00293.
- Crotwell, H. P., T. J. Owens, and J. Ritsema (1999), The TauP Toolkit: Flexible seismic travel-time and ray-path utilities, *Seismological Research Letters*, 70(April), 154–160, doi:10.1785/gssrl.70.2.154.
- Diez, A. (2013), Effects of cold glacier ice crystal anisotropy on seismic data, Ph.D. thesis, Karlsruher Institut für Technologie.
- Dziewoński, A. M., and D. L. Anderson (1981), Preliminary reference Earth model, *Physics of the Earth and Planetary Interiors*, 25(4), 297–356, doi:10.1016/0031-9201(81)90046-7.
- Ekström, G., A. M. Dziewoński, and J. M. Steim (1986), Single station CMT; Application to the Michoacan, Mexico, Earthquake of September 19, 1985, *Geophysical Research Letters*, 13(3), 173–176, doi:10.1029/GL013i003p00173.

- Global CMT Project (2017), GlobalCMT solution for the 2017/02/24 MW 5.9 LAKE TANGANYIKA REGION earthquake, doi:10.17611/DP/13444845.
- Golombek, M. P., W. B. Banerdt, K. L. Tanaka, and D. M. Tralli (1992), A prediction of Mars seismicity from surface faulting., *Science (New York, N.Y.)*, 258(5084), 979–81, doi:10.1126/science.258.5084.979.
- Grapenthin, R., and J. T. Freymueller (2011), The dynamics of a seismic wave field: Animation and analysis of kinematic GPS data recorded during the 2011 Tohoku-oki earthquake, Japan, *Geophysical Research Letters*, 38(18), doi:10.1029/2011GL048405.
- Hand, K. P., A. E. Murray, J. B. Garvin, and the Science Definition Team (2017), Report of the Europa Lander Science Definition Team, *Tech. rep.*, NASA, Pasadena, California.
- Hofgartner, J. D., A. G. Hayes, J. I. Lunine, H. Zebker, B. W. Stiles, C. Sotin, J. W. Barnes, E. P. Turtle, K. H. Baines, R. H. Brown, B. J. Buratti, R. N. Clark, P. Encrenaz, R. D. Kirk, A. Le Gall, R. M. Lopes, R. D. Lorenz, M. J. Malaska, K. L. Mitchell, P. D. Nicholson, P. Paillou, J. Radebaugh, S. D. Wall, and C. Wood (2014), Transient features in a Titan sea, *Nature Geoscience*, 7(7), 493–496, doi:10.1038/ngeo2190.
- Hogenboom, D., J. Kargel, J. Ganasan, and L. Lee (1995), Magnesium sulfate-water to 400 MPa using a novel piezometer: Densities, phase equilibria, and planetological implications, *Icarus*, 115(2), 258–277, doi:10.1006/icar.1995.1096.
- Iess, L., R. A. Jacobson, M. Ducci, D. J. Stevenson, J. I. Lunine, J. W. Armstrong, S. W. Asmar, P. Racioppa, N. J. Rappaport, and P. Tortora (2012), The tides of Titan, *Science*, 337(6093), 457–459.
- Iess, L., D. J. Stevenson, M. Parisi, D. Hemingway, R. A. Jacobson, J. I. Lunine, F. Nimmo, J. W. Armstrong, S. W. Asmar, M. Ducci, and P. Tortora (2014), The Gravity Field and Interior Structure of Enceladus, *Science*, 344(6179), 78–80.
- Igel, H. (2017), *Computational seismology: a practical introduction*, 1st ed., Oxford University Press, Oxford.
- Jacobson, R. A., P. G. Antreasian, J. J. Bordi, K. E. Criddle, R. Ionasescu, J. B. Jones, R. A. Mackenzie, M. C. Meek, D. Parcher, F. J. Pelletier, and others (2006), The Gravity Field of the Saturnian System from Satellite Observations and Spacecraft Tracking Data, *The Astronomical Journal*, 132(6), 2520–2526.
- Kedar, S., M. S. Longuet-Higgins, F. Webb, N. Graham, R. W. Clayton, and C. Jones (2008), The origin of deep ocean microseisms in the North Atlantic Ocean, *Proceedings of the Royal Society A: Mathematical, Physical and Engineering Sciences*, 464(2091), 777–793, doi:10.1098/rspa.2007.0277.
- Kennett, B. L. N. (2002), *The Seismic Wavefield: Interpretation of seismograms on regional and global scales*, Cambridge University Press.
- Khan, A., M. van Driel, M. Böse, D. Giardini, S. Ceylan, J. Yan, J. F. Clinton, F. Euchner, P. Lognonné, N. Murdoch, D. Mimoun, M. P. Panning, M. Knapmeyer, and W. Banerdt (2016), Single-station and single-event marsquake location and inversion for structure using synthetic Martian waveforms, *Physics of the Earth and Planetary Interiors*, doi:10.1016/j.pepi.2016.05.017.
- Kivelson, M. G., K. K. Khurana, C. T. Russell, M. Volwerk, R. J. Walker, C. Zimmer, R. Greeley, R. T. Pappalardo, J. W. Head, R. Greeley, G. V. Hoppa, B. R. Tufts, R. Greenberg, P. E. Geissler, R. Greenberg, M. G. Kivelson, K. K. Khurana, M. G. Kivelson, D. S. Colburn, R. T. Reynolds, F. M. Neubauer, F. M. Neubauer, D. J. Southwood, M. G. Kivelson, R. J. Walker, J. A. Slavin, F. M. Neubauer, A. J. Kliore, D. P. Hinson, F. M. Flasar, A. F. Nagy, T. E. Cravens, D. T. Hall, P. D. Feldman, M. A. McGrath, D. F. Strobel, J. Saur, D. F. Strobel, and F. M. Neubauer (2000), Galileo magnetometer measurements: a stronger case for a subsurface ocean at Europa., *Science (New York, N.Y.)*, 289(5483), 1340–3, doi:10.1126/science.289.5483.1340.
- Knapmeyer, M. (2003), Syntax Diagrams for the Body Wave Nomenclature with extensions for other terrestrial planets, in *Geophysical Research Abstracts*, , vol. 5, EGS-AGU-EGU Joint Assembly, Nice.

- Kovach, R. L., and C. F. Chyba (2001), Seismic Detectability of a Subsurface Ocean on Europa, *Icarus*, *150*(2), 279–287, doi:10.1006/icar.2000.6577.
- Krischer, L., T. Megies, R. Barsch, M. Beyreuther, T. Lecocq, C. Caudron, and J. Wassermann (2015), ObsPy: a bridge for seismology into the scientific Python ecosystem, *Computational Science & Discovery*, *8*(1), 014,003, doi:10.1088/1749-4699/8/1/014003.
- Kugler, S., T. Bohlen, S. Bussat, and G. Klein (2005), Variability of Scholte-wave Dispersion in Shallow-water Marine Sediments, *Journal of Environmental & Engineering Geophysics*, *10*(2), 203–218, doi:10.2113/JEEG10.2.203.
- Lee, S., M. Zanolin, A. M. Thode, R. T. Pappalardo, and N. C. Makris (2003), Probing Europa's interior with natural sound sources, *Icarus*, *165*, 144–167, doi:10.1016/S0019-1035(03)00150-7.
- Lee, W. H. K., and Y. Ben-Zion (2006), In Memory of Keiiti Aki, 1930–2005, *Pure and Applied Geophysics*, *163*(2-3), 617–618, doi:10.1007/s00024-005-0028-4.
- Lehmann, I. (1936), P', *Bureau Central Séismologique International, Série A, Travaux Scientifiques*, *14*, 87–115.
- Leng, K., T. Nissen-Meyer, and M. van Driel (2016), Efficient global wave propagation adapted to 3-D structural complexity: a pseudospectral/spectral-element approach, *Geophysical Journal International*, *207*(3), 1700–1721, doi:10.1093/gji/ggw363.
- Lewis, J. S. (1971), Satellites of the outer planets: Thermal models, *Science*, *172*, 1171–1172, doi:10.1126/science.172.3988.1127.
- Lognonné, P., F. Karakostas, L. Rolland, and Y. Nishikawa (2016), Modeling of atmospheric-coupled Rayleigh waves on planets with atmosphere: From Earth observation to Mars and Venus perspectives, *Journal of the Acoustical Society of America*, *140*(2), doi:10.1121/1.4960788.
- Lorenz, R. D., and A. G. Hayes (2012), The growth of wind-waves in Titan's hydrocarbon seas, *Icarus*, *219*(1), 468–475, doi:10.1016/j.icarus.2012.03.002.
- Lorenz, R. D., S. Kedar, N. Murdoch, P. Lognonné, T. Kawamura, D. Mimoun, and W. B. Banerdt (2015), Seismometer detection of dust devil vortices by ground tilt, *Bulletin of the Seismological Society of America*, *105*(6), 3015–3023, doi:10.1785/0120150133.
- McKinnon, W. B. (2015), Effect of Enceladus's rapid synchronous spin on interpretation of Cassini gravity, *Geophysical Research Letters*, *42*(7), 2137–2143, doi:10.1002/2015GL063384.
- Mohorovičić, A. (1909), Das Beben vom 8. Oktober 1909 (translated title), *Jahrbuch des meteorologischen Observatoriums in Zagreb*, *4*(1), 1–67.
- Nimmo, F., and R. Pappalardo (2016), Ocean Worlds in the Outer Solar System, *Journal of Geophysical Research: Planets*, doi:10.1002/2016JE005081.
- Nissen-Meyer, T., M. van Driel, S. C. Stähler, K. Hosseini, S. Hempel, L. Auer, A. Colombi, and A. Fournier (2014), AxiSEM: broadband 3-D seismic wavefields in axisymmetric media, *Solid Earth*, *5*(1), 425–445, doi:10.5194/se-5-425-2014.
- Nolet, G., and L. M. Dorman (1996), Waveform Analysis of Scholte Modes In Ocean Sediment Layers, *Geophysical Journal International*, *125*(2), 385–396, doi:10.1111/j.1365-246X.1996.tb00006.x.
- Oldham, R. D. (1906), The Constitution of the Interior of the Earth, as Revealed by Earthquakes, *Quarterly Journal of the Geological Society*, *62*(1-4), 456–475, doi:10.1144/GSL.JGS.1906.062.01-04.21.
- Panning, M. P., V. Lekic, M. Manga, F. Cammarano, and B. Romanowicz (2006), Long-period seismology on Europa: 2. Predicted seismic response, *Journal of Geophysical Research*, *111*(E12), E12,008, doi:10.1029/2006JE002712.
- Panning, M. P., ĀČ. Beucler, M. Drilleau, A. Mocquet, P. Lognonné, and W. B. Banerdt (2015), Verifying single-station seismic approaches using Earth-based data: Preparation for data return from the InSight mission to Mars, *Icarus*, *248*, 230–242, doi:10.1016/j.icarus.2014.10.035.
- Panning, M. P., S. C. Stähler, H.-H. Huang, S. Vance, S. Kedar, V. C. Tsai, and W. T. Pike (2017), The seismic noise environment of Europa, *Journal of Geophysical Research E*:

*Planets, submitted.*

- Peterson, J. (1993), Observations and Modeling of Seismic Background Noise, *Tech. rep.*, USGS, Albuquerque, New Mexico.
- Phillips, C. B., and R. T. Pappalardo (2014), Europa Clipper Mission Concept: Exploring Jupiter's Ocean Moon, *Eos, Transactions American Geophysical Union*, 95(20), 165–167, doi:10.1002/2014EO200002.
- Pike, W. T., S. Calcutt, I. M. Standley, A. G. Mukherjee, J. Temple, T. Warren, C. Charalambous, H. Liu, A. Stott, and J. B. McClean (2016), A Silicon Seismic Package (SSP) for Planetary Geophysics, in *Lunar and Planetary Science Conference*, vol. 47, p. 2081.
- Porco, C. C., P. Helfenstein, P. C. Thomas, A. P. Ingersoll, J. Wisdom, R. West, G. Neukum, T. Denk, R. Wagner, T. Roatsch, S. Kieffer, E. Turtle, A. McEwen, T. V. Johnson, J. Rathbun, J. Veverka, D. Wilson, J. Perry, J. Spitale, A. Brahic, J. A. Burns, A. D. DelGenio, L. Dones, C. D. Murray, and S. Squyres (2006), Cassini Observes the Active South Pole of Enceladus, *Science*, 311(5766).
- Press, F., and M. Ewing (1951), Propagation of elastic waves in a floating ice sheet, *Transactions, American Geophysical Union*, 32(5), 673, doi:10.1029/TR032i005p00673.
- Rauch, D. (1980), Experimental and Theoretical Studies of Seismic Interface Waves in Coastal Waters, in *Bottom-Interacting Ocean Acoustics*, edited by W. A. Kuperman and F. B. Jensen, pp. 307–327, Springer US, Boston, MA, doi:10.1007/978-1-4684-9051-0\_21.
- Ringler, A. T., and C. R. Hutt (2010), Self-Noise Models of Seismic Instruments, *Seismological Research Letters*, 81(6), 972–983, doi:10.1785/gssrl.81.6.972.
- Scholte, J. G. (1947), The range of existence of Rayleigh and Stoneley waves, *Geophysical Journal International*, 5(s5), 120–126, doi:10.1111/j.1365-246X.1947.tb00347.x.
- Schubert, G., J. D. Anderson, T. Spohn, and W. B. McKinnon (2004), Interior composition, structure and dynamics of the Galilean satellites, *Jupiter: The Planet, Satellites and Magnetosphere*, pp. 281–306.
- Storchak, D. A., J. Schweitzer, and P. Bormann (2003), The IASPEI standard seismic phase list, *Seismological Research Letters*, 74(6), 761–772.
- Thomas, P., R. Tajeddine, M. Tiscareno, J. Burns, J. Joseph, T. Lored, P. Helfenstein, and C. C. Porco (2016), Enceladus' measured physical libration requires a global subsurface ocean, *Icarus*, 264, 37–47, doi:10.1016/j.icarus.2015.08.037.
- Thomas, P. C. (2010), Sizes, shapes, and derived properties of the saturnian satellites after the Cassini nominal mission, *Icarus*, 208(1), 395–401.
- van Driel, M., L. Krischer, S. C. Stähler, K. Hosseini, and T. Nissen-Meyer (2015), Instantaneous global seismograms based on a broadband waveform database, *Solid Earth*, 6(2), 701–717, doi:10.5194/se-6-701-2015.
- Vance, S. D., M. Bouffard, M. Choukroun, and C. Sotin (2014), Ganymede's internal structure including thermodynamics of magnesium sulfate oceans in contact with ice, *Planetary and Space Science*, 96, 62–70, doi:10.1016/j.pss.2014.03.011.
- Vance, S. D., M. P. Panning, S. C. Stähler, B. G. Bills, F. Cammarano, V. C. Tsai, H.-H. Huang, W. T. Pike, and R. D. Lorenz, S. Kedar, C. Sotin, W. Banerdt (2017), Geophysical tests for habitability in ocean worlds, *Journal of Geophysical Research E: Planets, submitted*.
- Woodhouse, J. H. (1988), The Calculation of Eigenfrequencies and Eigenfunctions of the Free Oscillations of the Earth and the Sun, in *Seismological algorithms*, pp. 321–370.
- Wu, Y.-m., H.-y. Yen, L. Zhao, B.-s. Huang, and W.-t. Liang (2006), Magnitude determination using initial P waves : A single-station approach, *Geophysical Research Letters*, 33(March), 4–7, doi:10.1029/2005GL025395.
- Zebker, H., A. Hayes, M. Janssen, A. Le Gall, R. Lorenz, and L. Wye (2014), Surface of Ligeia Mare, Titan, from Cassini altimeter and radiometer analysis, *Geophysical Research Letters*, 41(2), 308–313, doi:10.1002/2013GL058877.